ChemComm
Chemical Communications

Accepted Manuscript

This article can be cited before page numbers have been issued, to do this please use: X. Pang, J. Ni, C. Shi, Y. Liao, X. Li, F. Guo, H. Yu and J. Han, *Chem. Commun.*, 2025, DOI: 10.1039/D5CC03644E.

ROYAL SOCIETY OF CHEMISTRY

rsc.li/chemcomm

View Article Online
DOI: 10.1039/D5CC03644E

COMMUNICATION

Charge Transfer Engineering of Carbon-Coated Porous ZnO to Enhance Oxygen Reduction for High-Efficiency Piezocatalytic H_2O_2 Production

Received 00th January 20xx,
Accepted 00th January 20xx

DOI: 10.1039/x0xx00000x

Xiyuan Pang [a], Jingren Ni [a], Chengdi Shi [a], Yuxuan Liao [a], Xiaoge, Li [a], Fan Guo [a], Hongjian Yu [a, *] and Jie Han [a]

Piezocatalysis holds remarkable potential for enabling eco-friendly and sustainable H_2O_2 production. In this study, a porous nanosheet-structured ZnO was synthesized via morphological engineering, demonstrating an enhanced surface area and superior stress responsiveness. Furthermore, a carbon layer derived from sodium lignosulfonate was introduced to construct a series of porous C/ZnO composites. The optimized catalyst effectively promotes the oxygen reduction reaction pathway, achieving a high H_2O_2 production rate of 4604.0 μmol·g^{-1}·h^{-1} in pure water without any cocatalysts or sacrificial agents. Combined experimental results and characterization analyses reveal that the carbon layer facilitates interfacial electron transfer and advances oxygen adsorption and activation, thereby substantially boosting catalytic performance. This work offers meaningful insights and a strategic reference for the development of advanced multifunction piezocatalytic systems.

Amidst the swift advancement of the global economy, the requirement for clean, eco-conscious, and sustainable energy resources is persistently escalating.[1] Hydrogen peroxide (H_2O_2), a prevalent eco-friendly oxidizing agent, has found extensive applications across diverse domains including chemical synthesis, healthcare, energy conversion, and environmental remediation.[2] The direct synthesis of H_2O_2 generally necessitates the use of noble metal catalysts and stringent reaction conditions, constraining its feasibility for large-scale industrial implementation.[3] Therefore, advancing a novel, energy-efficient, and sustainable H_2O_2 production technology with scalable potential has emerged as an urgent and pivotal challenge.[4]

Piezocatalysis is a promising catalytic approach that exploits the inherent piezoelectric effect of materials to induce and facilitate chemical transformations.[5, 6] When non-centrosymmetric crystalline piezoelectric materials are subjected to mechanical stress, structural deformation is induced, resulting in the formation of surface polarization charges, thereby enabling the conversion of mechanical energy into chemical energy.[7, 8] Numerous piezoelectric materials, such as $BaTiO_3$, $BiFeO_3$, ZnO, C_3N_4 and MoS_2, have been demonstrated to possess excellent piezocatalytic performance.[9-13] Among them, ZnO has emerged as a highly promising material for piezocatalytic applications, attributed to its remarkable excellent piezoelectric performance, good chemical stability, wide bandgap, and low cost.[14] Nevertheless, the practical utility of ZnO in piezocatalysis is hampered by several intrinsic limitations.[15] Hence, advanced material engineering and structural optimization strategies have become essential for boosting the piezocatalytic efficiency of ZnO.

Notably, various studies highlight the critical role of morphological design in determining the piezocatalytic efficiency of piezoelectric materials. In particular, porous nanosheet structures exhibit large specific surface areas and abundant exposed active sites, which facilitate the adsorption and activation of reactants.[16, 17] Moreover, their low-dimensional structure enhances the sensitivity of piezoelectric materials to subtle mechanical stimuli, while the presence of porous channels can induce strain engineering effects that further promote the generation of polarization charges, thereby improving catalytic performance.[18] In addition, coupling with carbon materials has emerged as a promising approach to address the intrinsic drawbacks of traditional piezocatalysts, such as inadequate catalytic efficiency, scarce active sites, and high activation energy requirements.[19] Owing to their highly developed porous frameworks and extensive surface areas, carbon-based materials provide abundant active interfaces that facilitate reactant adsorption and interfacial interaction among reaction species.[20] Additionally, their superior electronic conductivity supports effective charge separation and rapid migration of carriers, thus suppressing recombination and enhancing catalytic performance. Furthermore, the incorporation of carbon matrices can stabilize semiconductor nanophases by preventing particle aggregation and mitigating chemical degradation, thus significantly enhancing mechanical stability and long-term durability.[21] Despite notable advancements, the exploration of porous ZnO/carbon composites in piezocatalytic systems remains limited. Particularly, lignin, a naturally abundant, biodegradable, and renewable carbon feedstock, has been underutilized in the development of functional composite materials.[22] The fundamental mechanisms through which lignin-derived carbon components influence interfacial charge transfer and enhance piezocatalytic H_2O_2 production are still poorly understood, highlighting an essential research area that demands comprehensive elucidation.

[a] School of Chemistry and Chemical Engineering, Yangzhou University, Yangzhou 225002, Jiangsu, P. R. China. Email: yhj@yzu.edu.cn.

†Electronic Supplementary Information (ESI) available. See DOI: XXXXXXXXXXXXX

In this study, a series of porous C/ZnO composites were designed and synthesized based on porous ZnO with abundant active sites and stress-responsive characteristics, employing sodium lignosulfonate as a sustainable carbon source. The optimized carbon layer significantly promoted charge separation and accelerated interfacial electron transfer, thereby precisely modulating the piezocatalytic pathway for H_2O_2 generation. Benefiting from the boosting oxygen reduction pathway, the optimal composite achieves a H_2O_2 production rate as high as 4604.0 $\mu mol \cdot g^{-1} \cdot h^{-1}$ in pure water without the any cocatalysts or sacrificial agents, outperforming most advanced piezocatalysts. This work proposes a robust strategy for the rational design of high-performance piezocatalysts and underscores a scalable and environmentally benign approach for mechanical-driven H_2O_2 production.

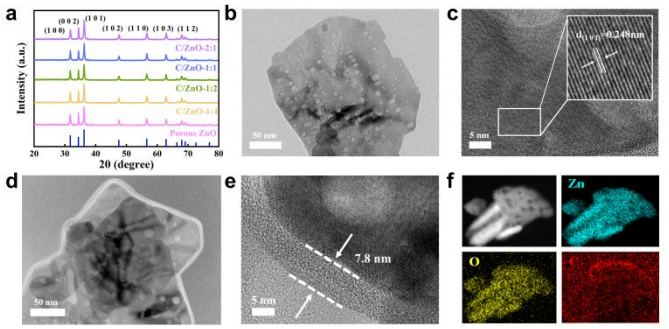

Fig. 1 a) XRD patterns of porous ZnO, C/ZnO-1:4, C/ZnO-1:2, C/ZnO-1:1 and C/ZnO-2:1. b, c) TEM image and HRTEM image of porous ZnO. d, e) TEM image and HRTEM image of C/ZnO-1:1. f) EDX elemental mappings for Zn, O and C of C/ZnO-1:1.

ZnO was synthesized via a facile precipitation route employing zinc acetate as the precursor. Subsequently, carbon derived from sodium lignosulfonate was introduced onto the ZnO substrate at various mass ratios through a combination of hydrothermal treatment and high-temperature calcination, resulting in the preparation of a series of C/ZnO composite catalysts. Full experimental details are outlined in the Supporting Information (Fig. S1). The XRD patterns of all samples matched well with ZnO (JCPDS No. 39-0233),[23] with no detectable impurity peaks observed (Fig. 1a). In addition, the Raman spectra (Fig. S2) exhibit characteristic carbon D (~1350 cm^{-1}) and G (~1580 cm^{-1}) bands, further indicating the successful synthesis of ZnO and the series of C/ZnO samples. Scanning electron microscopy (SEM) analysis demonstrates that both ZnO and C/ZnO possess similarly irregular stacked nanosheet structures (Fig. S3), suggesting that the incorporation of carbon does not significantly affect the inherent morphology or structural integrity of ZnO. Notably, transmission electron microscopy (TEM) observations reveal that the ZnO nanosheets display a well-defined porous structure (Fig. 1b), and the C/ZnO composite retains this porosity while featuring a uniformly coated carbon layer on the ZnO surface, with an estimated thickness of approximately 7.8 nm (Fig. 1d, e). High-resolution transmission electron microscopy (HRTEM) images of both ZnO and C-ZnO reveal an interplanar spacing of 0.248 nm, which corresponds to the (101) lattice plane of ZnO (Fig. 1c and Fig. S4). Moreover, elemental mappings distinctly demonstrate the presence of Zn, O, and C elements (Fig. 1f), thereby confirming the homogeneous distribution of the carbon layer on the ZnO surface.

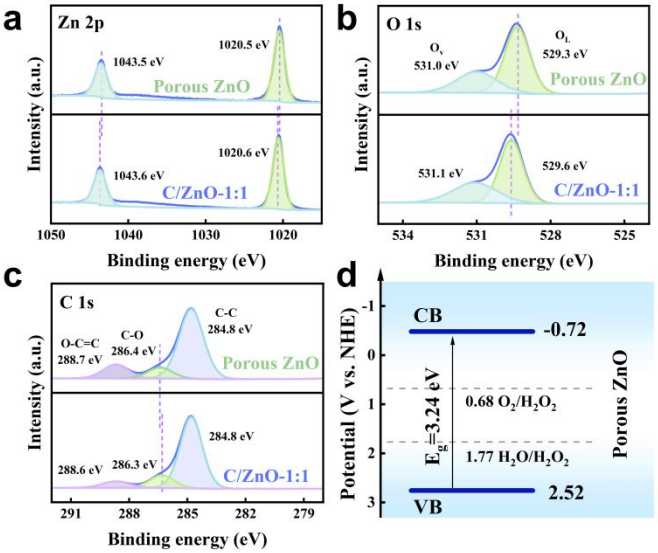

Fig. 2 XPS spectra of a) Zn 2p, b) O 1s, c) C 1s of porous ZnO and C/ZnO-1:1. d) The energy band structure diagrams of porous ZnO.

X-ray photoelectron spectroscopy (XPS) was employed to investigate the surface chemical composition and valence states of the catalysts. Porous ZnO exhibits a weak C peak at 284.4 eV, which may be attributed to the adsorption of atmospheric carbon species and carbon contamination onto the ZnO surface[14] (Fig. S5). Compared to pristine porous ZnO, C/ZnO-1:1 displays a significantly enhanced carbon signal at the same binding energy, suggesting the successful incorporation of a carbon onto the ZnO. The two distinct peaks of porous ZnO at 1020.5 eV and 1043.5 eV correspond to Zn $2p_{3/2}$ and Zn $2p_{1/2}$, respectively (Fig. 2a). Additionally, the peaks located near 529.3 eV and 531.0 eV are attributed to lattice oxygen and oxygen vacancies, respectively (Fig. 2b). Obviously, the O 1s and Zn 2p binding energies of C/ZnO-1:1 exhibit a positive shift relative to those of porous ZnO, suggesting a decrease in the electron cloud density around the Zn and O atoms following carbon incorporation. This observation further supports the role of porous ZnO as an electron donor, confirming the strong interfacial interaction between the carbon layer and porous ZnO, as well as the establishment of an efficient charge transfer pathway. In the C 1s spectrum of porous ZnO, the peaks near 284.8 eV, 286.4 eV, and 288.7 eV belong to C-C, C-O, and O-C=O, respectively (Fig. 2c). For C/ZnO-1:1, a negative shift in the C 1s binding energy is observed compared to porous ZnO, further supporting the role of carbon as an electron acceptor in this composite system. The UV/vis diffuse reflectance spectra (DRS) analysis reveals that the absorption edge of porous ZnO is located at around 375 nm, corresponding to a bandgap of 3.24 eV (Fig. S6). Combined with the Mott-Schottky analysis results, the band structure of porous ZnO is further elucidated (Fig. S7 and 2d), demonstrating that porous ZnO possesses sufficient redox capability to drive the H_2O_2 generation reaction.[24]

View Article Online
DOI: 10.1039/D5CC03644E

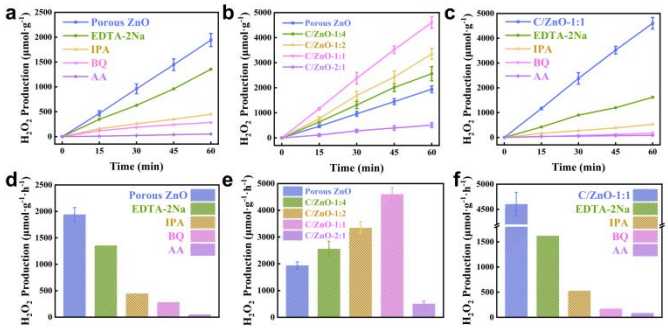

Fig. 3 a, d) H_2O_2 production and corresponding H_2O_2 production rates of porous ZnO with and without the addition of scavengers. b, e) H_2O_2 production and corresponding H_2O_2 production rates of porous ZnO, C/ZnO-1:4, C/ZnO-1:2, C/ZnO-1:1 and C/ZnO-2:1. c, f) H_2O_2 production and corresponding H_2O_2 production rates of C/ZnO-1:1 with and without the addition of different scavengers.

To highlight the advantage of the optimized structural design and effectual charge-transport behavior in enhancing the piezocatalytic performance, the H_2O_2 production activity of the prepared samples was assessed in pure water under ultrasonic vibration irradiation without the addition of cocatalystsor and sacrificial agents. Blank experiments confirmed that ultrasonic vibration in pure water generates only trace amounts of of H_2O_2 (Fig. S8). Notably, the porous ZnO exhibits outstanding piezocatalytic H_2O_2 production performance with a yield of 1942.1 $\mu mol \cdot g^{-1} \cdot h^{-1}$, which is approximately 1.68 times higher than that of ZnO nanosheets (1154.5 $\mu mol \cdot g^{-1} \cdot h^{-1}$) in Fig. S9. This result suggests that the optimized porous ZnO nanostructure demonstrates improved stress responsiveness and offers an increased availability of catalytic active sites. Additionally, the piezocatalytic H_2O_2 generation activity improves under increased ultrasonic power (Fig. S10). To further elucidate the catalytic mechanism and identify the active species involved in the piezocatalytic production of H_2O_2 over porous ZnO, scavenging experiments were conducted under 300 W ultrasonic irradiation using EDTA-2Na, isopropyl alcohol (IPA), p-benzoquinone (BQ), and ascorbic acid (AA) to trap holes (h^+), hydroxyl radicals (•OH), superoxide radicals ($\bullet O_2^-$), and electrons (e^-), respectively (Fig. 3a, d). The results demonstrated that the addition of BQ and AA significantly suppressed H_2O_2 generation, indicating that $\bullet O_2^-$ and e^- are the predominant active species. In contrast, EDTA-2Na and IPA exhibited minimal influence on H_2O_2 production, suggesting that h^+ and •OH play minor roles in the reaction. These findings indicate that the piezocatalytic generation of H_2O_2 on porous ZnO predominantly proceeds through an electron-mediated O_2 reduction pathway.

Based on the reaction pathway selectivity of porous ZnO in H_2O_2 production, sodium lignosulfonate, a widely available and cost-effective green carbon source, was employed to tailor the catalytic process. By harnessing the superior electron-conducting capabilities of carbon-based materials, the H_2O_2 generation pathway was further engineered and optimized. As illustrated in Figure 3b, e, C/ZnO-1:4, C/ZnO-1:2, and C/ZnO-1:1 all display enhanced H_2O_2 production performance compared to pure porous ZnO, with catalytic activity progressively improving as the carbon content increases. Notably, C/ZnO-1:1 exhibits the best performance, achieving an H_2O_2 yield up to 4604.0 $\mu mol \cdot g^{-1} \cdot h^{-1}$, which is approximately 2.37 times higher than that of porous ZnO. This remarkable performance also significantly outperforms most previously reported advanced piezocatalytic systems. (Fig. S11) However, further increasing the carbon content to C/ZnO-2:1 resulted in a sharp decline in H_2O_2 generation efficiency, even falling below that of the carbon-free ZnO. This is attributed to the excessive carbon layer potentially covering or blocking the porous structure of the ZnO nanosheets, thereby reducing the specific surface area and the exposure of active sites. Moreover, it may impede stress transmission and piezoelectric charge accumulation under ultrasonic irradiation, suppressing the catalytic performance. The active species trapping experiments on C/ZnO are consistent with those of pristine porous ZnO, suggesting that the introduction of the carbon layer does not alter the intrinsic reaction pathway for H_2O_2 generation (Fig. 3c, f). This improvement results from the substantially improved interfacial charge transfer between ZnO and the carbon phase within the composite, which enables more efficient separation of charge carriers. Consequently, this promotes accelerated oxygen reduction kinetics and ultimately elevates the overall catalytic performance. In addition, C/ZnO-1:1 shows consistent catalytic performances over 5 consecutive cycles (Fig. S12) and no significant structural changes after 10 h of ultrasonic treatment (Fig. S13), demonstrating enhanced stability and durability, which originates from the protective role of the carbon layer.

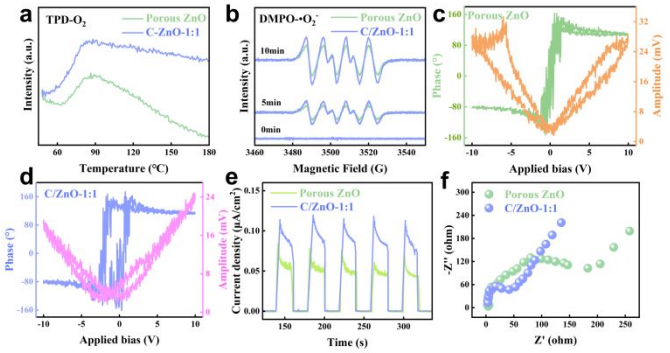

Fig. 4 a) TPD-O_2 profiles of porous ZnO and C/ZnO-1:1. b) ESR spin-trapping to identify the formation of $\bullet O_2^-$ radicals by porous ZnO and C/ZnO-1:1 under ultrasonic vibration. c, d) The butterfly amplitude loops and phase curves of porous ZnO and C/ZnO-1:1. e, f) Piezo-current intensity and electrochemical impedance spectra of porous ZnO and C/ZnO-1:1 under ultrasonic vibration.

O_2 temperature-programmed desorption (TPD-O_2) and *in situ* fourier transform infrared spectroscopy (FTIR) analysis were conducted to investigate the surface-active sites and the interaction behavior of O_2 on porous ZnO and C/ZnO-1:1. As illustrated in Figure 4a, C/ZnO-1:1 displays broader and more intense O_2 desorption peaks within the temperature range of 60-180 °C compared to porous ZnO. Moreover, C/ZnO1:1 demonstrates stronger O_2^- adsorption peaks at ~1169 cm^{-1} (Fig. S15). These results indicate that the formation of the carbon layer markedly enhances its oxygen adsorption capability, thereby facilitating the generation of abundant surface reactive oxygen species during the catalytic process. Furthermore, both porous ZnO and C/ZnO-1:1 exhibit characteristic DMPO-$\bullet O_2^-$ signals under ultrasonic irradiation, indicating that $\bullet O_2^-$ are the

predominant reactive species in both systems (Fig. 4b). Notably, the signal intensity of C/ZnO-1:1 is significantly higher than that of porous ZnO, suggesting that the introduction of the carbon layer effectively promotes the generation of $\bullet O_2^-$. Meanwhile, weak signals attributed to •OH are also detected, implying a minor contribution of •OH to the overall reaction (Fig. S14). These observations are in good agreement with the results from the active species capture experiment and O_2-TPD analysis. Porous ZnO and C/ZnO-1:1 present the typical butterfly-shaped amplitude loops and phase hysteresis, confirming that both porous ZnO and C/ZnO-1:1 possess distinct piezoelectric characteristics (Fig. 4c, d). Compared to porous ZnO, C/ZnO-1:1 displays a slightly reduced piezoelectric coefficient (d_{33}), which can be estimated from the amplitude loop. This reduction is attributed to the carbon layer impeding stress transmission. As presented in Figure 4e, f, C/ZnO-1:1 exhibits the highest piezo-current response and smallest arc radius, indicating that C/ZnO-1:1 possesses lower charge transfer resistance and higher charge separation and transfer efficiency under ultrasonic vibration.

According to the above experimental results, a possible mechanism for the piezocatalytic H_2O_2 production over porous ZnO and carbon-coated porous C/ZnO is proposed, as illustrated in Figure S16. For porous ZnO, ultrasonic vibrations induce lattice deformation, thereby generating an internal piezoelectric field. This built-in electric field drives the spatial separation of electrons and holes by facilitating their migration in opposite directions. The separated electrons subsequently interact with adsorbed O_2 molecules on the surface, leading to the formation of H_2O_2. Notably, the introduction of the carbon layer significantly increases the specific surface area and provides abundant active sites. Additionally, it facilitates the directional migration of electrons from ZnO to the carbon layer, further activating the adsorbed O_2 molecules and optimizing the oxygen reduction pathway. These synergistic effects collectively endow C/ZnO with superior piezocatalytic H_2O_2 production performance.

In summary, this study successfully synthesized porous ZnO nanosheets with ample active sites and stress sensitivity through morphology engineering and further developed a series of novel porous C/ZnO composite piezocatalysts by introducing a carbon layer derived from sodium lignosulfonate. Porous ZnO nanosheets exhibit improved piezocatalytic activity, achieving an H_2O_2 production rate of 1942.1 $\mu mol \cdot g^{-1} \cdot h^{-1}$, which is 1.68-fold higher than that of ZnO nanosheets (1154.5 $\mu mol \cdot g^{-1} \cdot h^{-1}$). Notably, the carbon layer effectively tailored the charge distribution in C/ZnO, promoting rapid interfacial electron transfer from ZnO to the carbon layer, which optimizes the H_2O_2 production path, enhances the oxygen reduction ability, and further elevates the catalytic reaction performance. The rationally engineered C/ZnO composite piezocatalyst achieved a significantly enhanced H_2O_2 production rate of 4604.0 $\mu mol \cdot g^{-1} \cdot h^{-1}$ in a pure water system, marking a 2.37-fold improvement over porous ZnO. This study establishes a robust framework for engineering high-performance porous C/ZnO piezocatalysts and provides a promising design concept for scalable H_2O_2 production driven by mechanical energy.

The authors gratefully acknowledge financial support from the National Natural Science Foundation of China (21922202, 21673202, 22302171 and 22272147), the Natural Science Foundation of Jiangsu Province (BK20220596) , and the Priority Academic Program Development of Jiangsu Higher Education Institutions.

Data availability

The data supporting this article have been included as part of the ESI. †

Conflicts of interest

There are no conflicts to declare.

Notes and references

1 L. Liu, H. Huang, Z. Chen, H. Yu, K. Wang, J. Huang, H. Yu and Y. Zhang, *Angew. Chem. Int. Ed.*, 2021, **60**, 18303-18308.
2 W. Chi, Y. Dong, B. Liu, C. Pan, J. Zhang, H. Zhao, Y. Zhu and Z. Liu, *Nat. Commun.*, 2024, **15**, 49663.
3 Z. Chen, D. Yao, C. Chu and S. Mao, *Chem. Eng. J.*, 2023, **451**, 138489.
4 P. Wei, L. Jiaxin, L. Xiaoqing, W. Liqun, Y. Lichang, T. Haotian, H. Feng and L. Ji, *Nat. Commun.*, 2023, **14**, 4430.
5 S. Lin, Q. Wang, H. Huang and Y. Zhang, *Small*, 2022, **18**, e2200914.
6 C. C. Jin, D. M. Liu and L. X. Zhang, *Small*, 2023, **19**, e2303586.
7 C. Hu, S. Tu, N. Tian, T. Ma, Y. Zhang and H. Huang, *Angew. Chem. Int. Ed.*, 2021, **60**, 16309-16328.
8 W. Jima, F. Yuheng, H. Guo-Hua, W. Shan and X. Chuanxi, *Polymers*, 2021, **13**, 2037.
9 Y. Fu, Z. Ren, J. Wu, Y. Li, W. Liu, P. Li, L. Xing, J. Ma, H. Wang and X. Xue, *Appl. Catal. B*, 2021, **285**, 119785.
10 E. Lin, N. Qin, J. Wu, B. Yuan, Z. Kang and D. Bao, *ACS Appl. Mater. Interfaces*, 2020, **12**, 14005-14015.
11 L. Bai, H. Huang, S. Zhang, L. Hao, Z. Zhang, H. Li, L. Sun, L. Guo, H. Huang and Y. Zhang, *Adv. Sci.*, 2020, **7**, 2001939.
12 Z. Kang, K. Ke, E. Lin, N. Qin, J. Wu, R. Huang and D. Bao, *J. Colloid Interface Sci.*, 2022, **607**, 1589-1602.
13 D. Liu, C. Jin, F. Shan, J. He and F. Wang, *ACS Appl. Mater. Interfaces*, 2020, **12**, 17443-17451.
14 Y. Wen, W. Liu, P. Wang, H. Che, C. Tang, B. Liu and Y. Ao, *Adv. Funct. Mater.*, 2023, **33**, 202308084.
15 Y. Wu, D. Yang, Y. Zhang, S. Jiao, W. Tang, Z. Wang, N. Wu, Y. Wang, W. Zhong, A. Zhang, J. Hao, H.-L. Cai and X. S. Wu, *Chem. Eng. J.*, 2022, **439**, 135640.
16 X.-C. Li, J.-H. Wang, T.-T. Huang, Y. Hu, X. Li, D.-J. Wang, W.-W. Wang, K. Xu, C.-J. Jia, H. Dong, G. Li, C. Li and Y.-W. Zhang, *Nat. Commun.*, 2025, **16**, 1234.
17 S. Tu, Y. Guo, Y. Zhang, C. Hu, T. Zhang, T. Ma and H. Huang, *Adv. Funct. Mater.*, 2020, **30**, 2005158.
18 L. Shichang, M. Farid, C. Jinmiao, W. Xinfei, W. Shaolei, Y. Junyi, Y. Ming, C. Xuxu, Y. Xinhua and Z. Yunlei, *Nanomicro Lett.*, 2024, **16**, 45.
19 P. Shen, P. Yin, Y. Zou, M. Li, N. Zhang, D. Tan, H. Zhao, Q. Li, R. Yang, B. Zou and B. Liu, *Adv. Mater.*, 2023, **35**, e2212172.
20 Y. Chen, J. Huang, Z. Chen, C. Shi, H. Yang, Y. Tang, Z. Cen, S. Liu, R. Fu and D. Wu, *Adv. Sci.*, 2022, **9**, e2103477.
21 C. Hu and L. Dai, *Adv. Mater.*, 2019, **31**, e1804672.
22 X. Liu, C. Chen, Y. Cao, C. Peng, J. Fang, H. Wang, W. Wu, G. Lyu and H. Li, *Colloids Surf. A*, 2023, **678**, 132505.
23 M. K. Hossain, A. A. Al-Saadi and F. Khan, *Opt. Laser Technol.*, 2025, **189**, 113062.
24 K. Wang, X. Liu, J. Chen, J. Luo, C. Yang and J. Wang, *Angew. Chem. Int. Ed.*, 2022, **61**, e202110429.

View Article Online
DOI: 10.1039/D5CC03644E

Data availability

The data supporting this article have been included as part of the ESI.